

Impact of diffusion on transverse dispersion in two-dimensional ordered and random porous media

Dzmitry Hlushkou,¹ Stanislaw Piatrusha,^{2,3} and Ulrich Tallarek^{1,*}

¹*Department of Chemistry, Philipps-Universität Marburg, Hans-Meerwein-Strasse 4, 35032 Marburg, Germany*

²*Laboratory of Electron Kinetics, Institute of Solid State Physics, Russian Academy of Sciences, Academician Ossipyan Strasse 2, 142432 Chernogolovka, Russia*

³*Laboratory of Topological Quantum Phenomena in Superconducting Systems, Moscow Institute of Physics and Technology, Institutskiy Per. 9, 141700 Dolgoprudny, Russia*

(Received 27 February 2017; published 19 June 2017)

Solute dispersion in fluid flow results from the interaction between advection and diffusion. The relative contributions of these two mechanisms to mass transport are characterized by the reduced velocity ν , also referred to as the Péclet number. In the absence of diffusion (i.e., when the solute diffusion coefficient $D_m = 0$ and $\nu \rightarrow \infty$), divergence-free laminar flow of an incompressible fluid results in a zero-transverse dispersion coefficient ($D_T = 0$), both in ordered and random two-dimensional porous media. We demonstrate by numerical simulations that a more realistic realization of the condition $\nu \rightarrow \infty$ using $D_m \neq 0$ and letting the fluid flow velocity approach infinity leads to completely different results for ordered and random two-dimensional porous media. With increasing reduced velocity, D_T approaches an asymptotic value in ordered two-dimensional porous media but grows linearly in disordered (random) structures depending on the geometrical disorder of a structure: a higher degree of heterogeneity results in a stronger growth of D_T with ν . The obtained results reveal that disorder in the geometrical structure of a two-dimensional porous medium leads to a growth of D_T with ν even in a uniform pore-scale advection field; however, lateral diffusion is a prerequisite for this growth. By contrast, in ordered two-dimensional porous media the presence of lateral diffusion leads to a plateau for the transverse dispersion coefficient with increasing ν .

DOI: [10.1103/PhysRevE.95.063108](https://doi.org/10.1103/PhysRevE.95.063108)

I. INTRODUCTION

Understanding the transport of solutes in porous media is important in many industrial and environmental processes, including catalysis, chromatography, ground water contamination and remediation, oil recovery, and nuclear waste disposal [1–5]. The spreading of passive solutes in fluid flow through a porous medium results from the interplay of diffusion and advection [6]. Even laminar flow in a porous medium is characterized by spatial fluctuations of the velocity within and between individual pores and by tortuous pathways that the fluid follows. This leads to different migration velocities of solutes in different flow streamlines, which is additionally affected by shearing, splitting, and merging of fluid streamlets. Diffusion acts as a mechanism providing exchange (mixing) between solute molecules travelling along different streamlines in individual pores. The resulting spreading of solutes is referred to as hydrodynamic dispersion. Thus, the three essential processes giving rise to solute spreading in fluid flow through porous media are diffusion, intrinsic mechanical dispersion due to flow heterogeneity at the interpore scale, and diffusively coupled mechanical dispersion at the intrapore scale [7].

At the macroscopic scale (that is many times larger than the dimensions of a single pore), the hydrodynamic dispersion in fluid flow through porous media is traditionally modeled by the advection–diffusion equation [6]. The basic idea of this approach is to consider dispersion processes as an anisotropic diffusion-like spreading of the solute concentration characterized by macroscopic (effective) transport coefficients, i.e.,

the longitudinal dispersion coefficient D_L and the transverse dispersion coefficient D_T in the direction of and normal to the average fluid flow, respectively. Dispersion processes in porous media have also been analyzed with a wide variety of theoretical techniques and geometrical models. For example, Brenner [8] used the method of spatial moments to develop a general theory for dispersion in granular and sintered, spatially periodic porous media and showed that in the long-time limit the dispersion of tracer particles obeys the advection–diffusion equation. The multiple-scale expansion or homogenization method was applied to determine dispersion coefficients in spatially periodic porous media [9]. The method of volume-averaging [6] was employed to derive proper forms of the transport equation and to calculate the dispersion coefficients in ordered and random porous media [10–14]. Koch and Brady [15] used an ensemble-averaging approach to obtain a macroscopic equation of mass conservation. They analyzed the derived transport equation in the long-time limit and revealed three contributions to dispersion in fluid flow through a bed of fixed spheres: (i) intrinsic mechanical dispersion due to the stochastic velocity fluctuations induced by the randomly positioned bed particles; (ii) retention of the diffusing species in permeable particles or in regions with closed streamlines, from which the species can escape only by diffusion; and (iii) the presence of the diffusive boundary-layer near the solid–liquid interface. Van Milligen and Bons [16] proposed a heuristic model of dispersion based on the assumption that transport in each of the pore channels traversed by a tracer is dominated by either diffusion or mechanical dispersion. The developed expressions for D_L and D_T include three free parameters (a critical velocity and two geometric proportionality constants), which depend on the porous medium properties. A fit of the proposed expressions

*tallarek@staff.uni-marburg.de

to an ample collection of experimental data revealed good accuracy of the model for a wide range of flow velocities. However, values of the parameters in the proposed model can be only determined from fitting to experimental data.

Over the past decades, the modeling of solute transport and dispersion in porous media has been performed also with a pore network approach, where a porous material is represented as an interconnected network of channels and/or pores [17–37]. In these models, the complex geometry of the void space in porous media is replaced with a simplified and “equivalent” pore network. Elements of this network are typically assigned to simple shapes, e.g., spheres and cylinders, amenable to analytical treatment. This approximation allows to reduce computational efforts in simulations of transport phenomena. The results obtained with a pore-network approach show that the morphology of a porous medium strongly affects dispersion. However, the main challenge arising due to the above simplification is to identify and preserve essential geometric and topological features of the real void space, which are relevant to both advective and diffusive transport.

The lack of detailed information on the geometrical structure of real porous media, which is required for a direct pore-level modeling of transport phenomena, can be overcome by physical reconstruction of the pore space morphology. Several experimental techniques, such as nuclear magnetic resonance imaging, x-ray tomography, confocal laser scanning microscopy, and scanning transmission electron microscopy, were used for the acquisition of information on the three-dimensional geometrical structure of the void space in a variety of natural and synthetic porous media. They include sandstones, packed beds, reservoir rocks, and chromatographic monoliths. Then, this information was employed for pore-level numerical simulations of mass transport in these materials [38–51]. However, this simulation approach is computationally expensive and commonly requires the use of high-performance parallel computational systems (supercomputers).

Results obtained with the aforementioned theoretical and numerical approaches indicate that D_L and D_T depend on both the geometrical structure of the porous medium and the reduced flow velocity $\nu = uG/D_m$ (also known as the Péclet number), where u is the average velocity through the medium, G is a characteristic length of the medium (e.g., the grain size or the mean interstitial void size), and D_m is the free diffusion coefficient of the species in the bulk fluid. Because the geometrical structure of the void space in a three-dimensional random porous medium is complex, studies of dispersion in porous media are frequently based on replacing the random geometry by a periodic structure and on subsequent reduction of the three-dimensional problem to a two-dimensional one. Though these simplifications allow us to reduce significantly computational expenses and the theoretical complexity of the problem, the applicability of results obtained with this simplified approach to random three-dimensional porous media is questionable.

It is well established that advective transport in two- and three-dimensional porous media is fundamentally different [52]. In three-dimensional porous domains, the flow streamlines of the incompressible fluid can twist around and pass each other without intersecting. By contrast, the

streamlines of a steady-state divergence-free flow field can never pass each other in two dimensions. This, for example, is manifested in completely different behaviors of the transverse dispersion coefficient in two- and three-dimensional porous media. Attinger *et al.* [53] showed theoretically that for pure advective transport ($D_m = 0$) D_T is finite in three dimensions and zero in two dimensions. The unphysical assumption of $D_m = 0$ immediately results in $\nu \rightarrow \infty$, independent of the flow velocity u . However, the condition $\nu \rightarrow \infty$ can also be realized with the assumption of a finite D_m and $u \rightarrow \infty$. Brenner [8] and Koch *et al.* [54] pointed out that molecular diffusivity must always be accounted for in hydrodynamic dispersion studies. This requirement arises not only because diffusion is one of the principal transport mechanisms, but also due to its coupling with advection.

In the present paper, we investigate numerically the transverse dispersion coefficient in a hexagonal array and in disordered arrays of solid (i.e., impermeable), equal discs. While the hexagonal disc array represents a two-dimensional porous medium with a regular geometrical structure, the disordered arrays mimic random two-dimensional porous media. Their structural disorder was generated through a distortion of the hexagonal array by introducing contacting discs. Complementary, a completely random arrangement of the discs was realized by adapting a Jodrey–Tory algorithm [55]. Advective–diffusive transport of passive tracers was simulated by two different approaches. The first one is based on a random-walk particle-tracking (RWPT) technique. At the first stage, the pore-scale velocity field of an incompressible Newtonian fluid in laminar flow was calculated with a lattice-Boltzmann method (LBM). Then, a large number of point-like tracers was distributed in the void space. The tracer displacements during each elementary time step were determined as the sum of two independent contributions due to advection (determined by the local flow velocity) and diffusion (determined by D_m). This comprehensive approach to the simulation of advective–diffusive transport accounts for the heterogeneity of the velocity field at the intra- and inter-pore scales of a porous medium. The second, simplified simulation approach we used in this study is based on modifications of the Galton-board model [56] and its successor, the Simpson model [57]. With this approach, the geometrical structure of a porous medium is represented by a set of rectangular void and solid cells. Velocity in the void cells is assumed to be uniform and along the average flow direction through the medium. We show that, regardless of the aforementioned geometrical and physical simplifications, the proposed modification of the Simpson model reproduces qualitatively (and for the hexagonal array even quantitatively) the behavior of D_T as a function of the reduced velocity. The main purpose of the simplified model, in addition to the LBM–RWPT approach, has been to eliminate any factors, except for the geometrical disorder, that eventually affect the dependence of D_T on ν in random porous media.

The two simulation approaches have been used to study the behavior of D_T in the ordered and disordered or random two-dimensional structures at high reduced velocities when the contribution of diffusion to mass transport becomes much smaller than the advective contribution, reflecting the conditions $\nu \rightarrow \infty$ and $D_m \neq 0$, and to analyze the effect of order/disorder in the studied system on D_T . The article is

organized as follows. First, a brief introduction into the LBM and RWPT techniques as well as the results obtained with these approaches for the hexagonal and random arrays of hard discs are presented. Afterwards, the Galton-board and Simpson models are described with an analysis of their shortcomings. Then, we present our modification of the Simpson model. Results with this modification for the hexagonal disc array are compared with LBM–RWPT simulations and experimental data. In addition, we employ the modified Simpson model to evaluate the transverse dispersion coefficient in disordered disc arrays as a function of the reduced velocity. We show that in the presence of diffusion the behavior of D_T is different in ordered and disordered two-dimensional porous media: With increasing reduced velocity, the transverse dispersion coefficient approaches an asymptotic value in ordered two-dimensional porous media, while it grows linearly in disordered (random) structures. These results refute the assumption frequently met in the literature that a leveling-off in D_T at high ν must be observed both with ordered and disordered two-dimensional porous media due to the inherent properties of incompressible fluid flow in two-dimensional systems [58–62]. Though our study focuses on the analysis of transverse dispersion due to advective–diffusive transport in two-dimensional porous media, we finalize our discussion of the results by a comparison with data obtained for three-dimensional ordered and random porous media.

II. LATTICE-BOLTZMANN AND RANDOM-WALK PARTICLE-TRACKING METHODS

The lattice-Boltzmann method (LBM) is a kinetic approach with discrete space and time, based on resolving the Boltzmann equation instead of the Navier–Stokes equation to compute the flow velocity field. Among the advantages of the LBM are its inherent parallelism (supporting the implementation at high-performance computational systems) and the capability to handle topologically complex solid–liquid interfaces like in random porous media. With this approach, the hydrodynamics is simulated by tracking the time-evolution of fictitious particles that are confined to a cubic lattice and move with discrete velocity \mathbf{e}_α during discrete time steps along lattice links. The particle distribution function $f_\alpha(\mathbf{r}, t)$ determines the probability of finding a particle with velocity \mathbf{e}_α at lattice site \mathbf{r} and time t . The values of the velocities \mathbf{e}_α are chosen such that in one time step δt_{LB} a particle moves along a lattice link from one lattice node to its neighbor. Next, the particle distributions functions at each time step are redistributed according to the collision operator. Here, we used the Bhatnagar–Gross–Krook collision operator and the evolution equation $f_\alpha(\mathbf{r}, t)$ is [63]

$$f_\alpha(\mathbf{r} + \delta t_{\text{LB}} \mathbf{e}_\alpha, t + \delta t_{\text{LB}}) = f_\alpha(\mathbf{r}, t) - \frac{f_\alpha(\mathbf{r}, t) - f_\alpha^{\text{eq}}(\mathbf{r}, t)}{\tau}, \quad (1)$$

where f_α^{eq} is the equilibrium distribution function and τ is the relaxation parameter, which is related to the fluid viscosity by $\eta = (2\tau - 1)/6$ [64]. The local fluid density $\rho(\mathbf{r}, t)$ and velocity $\mathbf{u}(\mathbf{r}, t)$ are determined by the first-order and second-

order moments of the particle distribution functions:

$$\rho(\mathbf{r}, t) = \sum_\alpha f_\alpha(\mathbf{r}, t) \quad (2)$$

and

$$\mathbf{u}(\mathbf{r}, t) = \frac{1}{\rho(\mathbf{r}, t)} \sum_\alpha \mathbf{e}_\alpha f_\alpha(\mathbf{r}, t). \quad (3)$$

Employing the Chapman–Enskog expansion, the equilibrium distribution functions in Eq. (1) can be calculated according to the following expression [65]:

$$f_\alpha^{\text{eq}}(\mathbf{r}, t) = w_\alpha \rho \left[1 + \frac{\mathbf{e}_\alpha \mathbf{u}}{c_s^2} + \frac{(\mathbf{e}_\alpha \mathbf{u})^2}{2c_s^4} - \frac{\mathbf{u} \mathbf{u}}{2c_s^2} \right], \quad (4)$$

where c_s is the speed of sound and w_α are weight factors that depend on the geometry of the employed lattice. We used the D_3Q_{19} lattice [66,67], a cubic lattice with 18 links at each lattice node, which can be obtained by projecting the four-dimensional face-centered hypercubic lattice onto three-dimensional space. In the D_3Q_{19} lattice each node is connected to its six nearest and twelve diagonal neighbors. It can be shown that Eq. (4) with weight factors of $w_\alpha = 1/3$ (for $\alpha = 0$), $w_\alpha = 1/18$ (for $\alpha = 1, 3, 5, 7, 10, 13$), and $w_\alpha = 1/36$ (for $\alpha = 2, 4, 6, 8, 9, 11, 12, 14, 15, 16, 17, 18$; conventional numbering for links in a D_3Q_{19} lattice) properly recovers the Navier–Stokes equation [68]. To realize the no-slip velocity boundary condition, a halfway bounce-back rule was implemented at the solid–liquid interface [69]. During the past decade, the LBM was extensively used to calculate pore-scale velocity fields in porous media. Recently, its accuracy was validated and confirmed by a direct comparison of the hydraulic permeability simulated in physically reconstructed monolithic porous media with experimental values obtained for these materials [43,70].

In this study, we used the LBM to calculate pore-scale flow velocity fields in the void space of hexagonal and random disc arrays with a solid volume fraction of $\phi = 0.6$, assuming a laminar flow regime. The random array of discs (which contains ca. 4.6×10^7 discs with diameter d_p) was generated by the Jodrey–Tory algorithm [55] in a rectangular domain with dimensions of $2000d_p \times 30000d_p$ and periodic boundary conditions. Implementation of periodic boundaries assumes that the disc position on one side of the domain influences the positions of discs at the opposite side. Then, hexagonal and random arrays were discretized on a uniform lattice with a lattice spacing of $d_p/100$, which was used for the LBM simulations of fluid flow. It has been shown that this grid resolution is sufficient for accurate LBM flow simulations in random sphere packings [71].

In the next step, the computed flow fields were used to simulate advective–diffusive transport of inert point-like tracers with the RWPT method [9]. It is based on the equivalence of the advective–diffusive equation,

$$\frac{\partial c}{\partial t} + \mathbf{u} \cdot \nabla c = D_m \nabla^2 c, \quad (5)$$

where c denotes concentration, and the stochastic differential equation describing the random walk of a tracer in an advection velocity field [72]. In two dimensions, the discrete form of the

stochastic differential equation is

$$\mathbf{r}(t + \delta t_{RW}) = \mathbf{r}(t) + \mathbf{u}(\mathbf{r})\delta t_{RW} + \xi\sqrt{4D_m\delta t_{RW}}, \quad (6)$$

where $\mathbf{r}(t)$ stands for the tracer position at time t , δt_{RW} is the elementary time step of the random walk, and ξ is a vector with a random orientation and a length governed by a Gaussian distribution with zero mean and unity variance. Algorithmically, Eq. (6) was realized to simulate advective–diffusive transport of tracers in the interstitial void space of the arrays as follows. Initially, a large number of tracers N_{tr} (10^6) were uniformly distributed at random positions in the void space. Then, at each elementary time step δt_{RW} , the displacement of a tracer was determined as the sum of advective and diffusive contributions represented by the second and third terms on the right-hand side of Eq. (6), respectively. The advective contribution was calculated with the velocity vector \mathbf{u} from the nearest node of the lattice used to simulate the velocity field by the LBM. The time step δt_{RW} was defined so that the average displacement did not exceed $d_p/200$. A multiple-rejection scheme was implemented to restrict the movement of tracers to the void space [73]. The time-evolution of tracer coordinates was monitored and the transverse dispersion coefficient determined from

$$D_T = \frac{1}{2N_{tr}} \frac{d}{dt} \sum_{a=1}^{N_{tr}} (\Delta y_a - \langle \Delta y \rangle)^2, \quad (7)$$

where Δy_a and $\langle \Delta y \rangle$ are, respectively, the transverse displacement of the a th tracer and the average transverse displacement of the tracer ensemble.

In recent years, the RWPT technique combined with the LBM was extensively used to study hydrodynamic dispersion in porous media [42,71,74–84]. The comparison with experimental data confirmed that this approach allows to determine longitudinal and transverse dispersion coefficients with high accuracy [84]. The above numerical methods presented in this section were realized as parallel codes in C/C++ languages and implemented on an IBM BlueGene/Q supercomputer (Jülich Supercomputing Center, Forschungszentrum Jülich, Jülich, Germany). The calculation of a steady-state velocity field required approximately 2 h at 256 processors, and the simulation of hydrodynamic dispersion for 30 values of the reduced flow velocity took about 4 h at 256 processors.

Figure 1 shows the transverse dispersion coefficient as a function of the reduced flow velocity $\nu = ud_p/D_m$ obtained for the hexagonal and random arrays of discs using the LBM–RWPT approach. The results in Fig. 1 demonstrate that, in contrast to the theoretical prediction for pure advective transport (when $D_m = 0$) [53], D_T is not zero even at very high values of ν , at which advection is the (by far) dominating transport mechanism. This means that the diffusive contribution to mass transport, no matter how small compared to the advective contribution, cannot be neglected in a realistic analysis of hydrodynamic dispersion in porous media. In addition, the behavior of D_T for $\nu \rightarrow \infty$ is different for ordered and random array; while D_T in the hexagonal array levels off, it continues to grow with ν in the random array. Thus, the structural order/disorder is another key parameter that determines the behavior of the transverse dispersion coefficient at high reduced velocities. We discuss these results in detail in the last

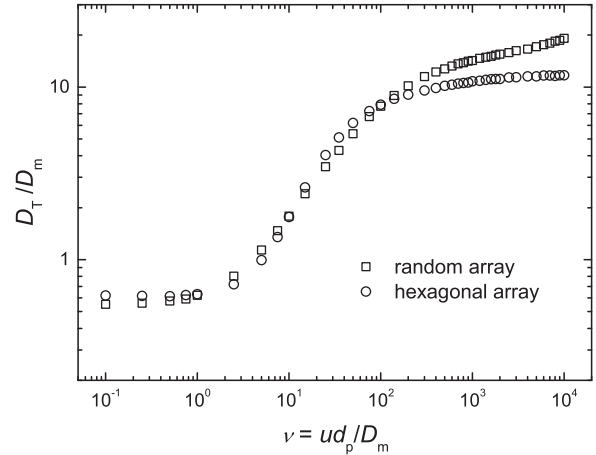


FIG. 1. Transverse dispersion coefficient D_T normalized by the free diffusion coefficient D_m as a function of the reduced velocity $\nu = ud_p/D_m$, obtained by the LBM–RWPT approach, for a hexagonal and a random array of equal discs with solid volume fraction $\phi = 0.6$. The diameter of the discs d_p is 10^{-5} m and the free diffusion coefficient of the tracers D_m is 10^{-9} m² s⁻¹.

section. In the next sections, we present a simplified model of transverse dispersion in two-dimensional porous media and show that it allows to reproduce the functional behavior of D_T in the ordered and disordered structures obtained with the LBM–RWPT approach (Fig. 1). This signifies that geometrical disorder in the presence of diffusion results in an increase of D_T with ν even in a divergence-free and pore-scale uniform flow field in a two-dimensional porous medium.

III. MODIFIED SIMPSON MODEL

Though a spatially periodic porous medium is an idealization of real porous materials, this geometrical model is of theoretical interest, because the problem of determining the dispersion coefficients in such simplified media may be reduced to the investigation of transport processes in a single unit cell [8]. The simplest and most studied periodic geometrical model of a porous medium is a hexagonal array of infinitely long cylindrical pillars, which can be reduced to a two-dimensional hexagonal array of discs [Fig. 2(a)]. This configuration closely resembles the Galton board, a device constructed to demonstrate experimentally that the normal distribution approximates the binominal distribution. If a falling ball, when it hits a pin, can bounce to the left or to the right with probability 0.5, then the probability $f(i, n)$ to find a ball in the i th compartment of the n th layer of the Galton board [Fig. 2(b)] is governed by the binominal distribution

$$f(i, n) = \frac{n!}{(n-i)!i!} 2^{-n}, \quad 0 \leq i \leq n. \quad (8)$$

The Galton-board model can be applied to describe transverse dispersion in a hexagonal array of pillars or discs [Fig. 2(a)] under the assumption of a uniform velocity in the interstitial void space. With this approach, transverse dispersion is treated as a random-walk process composed of successive and equiprobable displacements of a tracer by a

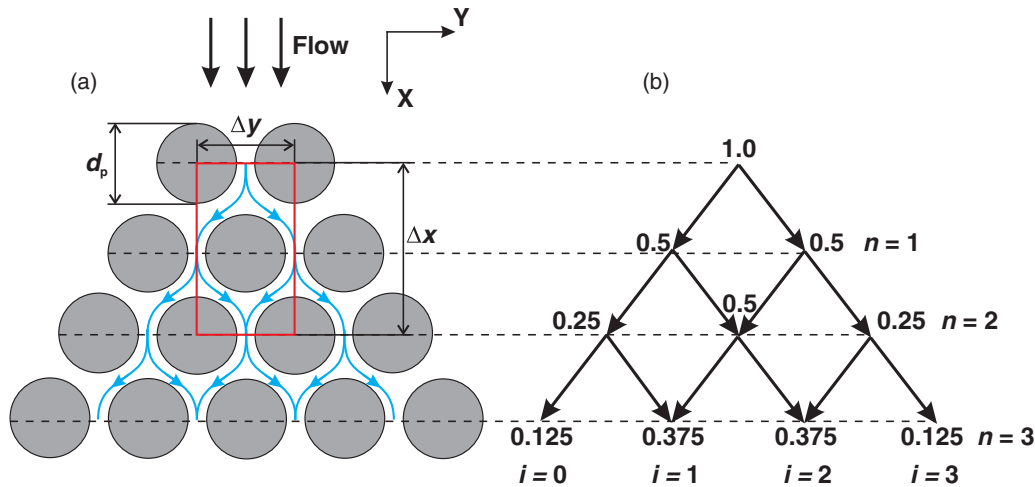


FIG. 2. (a) Hexagonal array of discs (d_p is the disc diameter, Δx and Δy are the longitudinal and transverse dimensions, respectively, of the unit cell). Blue lines illustrate the splitting and merging of flow streamlines. The red rectangle indicates a unit cell. (b) Schematic illustration of the probability distribution to find a falling ball in the i th compartment of the n th layer of the Galton board. This probability is governed by the binominal distribution [Eq. (8)]. The arrows show possible displacements of the ball, which occur with frequency $1/\Delta t$.

distance $\Delta y/2$ along the either positive or negative directions of the y -axis. Transverse displacements are associated with the splitting streamlines of the flow velocity upstream of every disc. Each transverse displacement is accompanied by a displacement Δx along the axial direction, i.e., the average flow direction through the array. These displacements occur with frequency $1/\Delta t = 2u/\Delta x$, where u is the axial velocity. The geometrical parameters Δx and Δy describe the unit cell in a hexagonal disc array [red rectangle in Fig. 2(a)]. The variance of the transverse displacement of the tracer from its original position after n displacements is given by [85]

$$\sigma_{T,n}^2 = n \frac{\Delta y^2}{4}. \quad (9)$$

The transverse dispersion coefficient can be determined by the method of moments [17,86,87] as

$$D_T = \frac{1}{2} \frac{\sigma_{T,n}^2}{t_n}, \quad (10)$$

where $t_n = n\Delta t$ is the time required to perform n displacements. Substituting Eq. (9) into Eq. (10), we get

$$D_T = \frac{1}{4} \frac{\Delta y^2}{\Delta x} u. \quad (11)$$

For a hexagonal array of discs or pillars, the values of Δx and Δy can be determined from the diameter of the discs d_p and the solid volume fraction ϕ as

$$\Delta x = d_p \left(\frac{\pi \sqrt{3}}{\phi \sqrt{2}} \right)^{1/2}, \quad (12)$$

$$\Delta y = d_p \left(\frac{\pi}{2\phi \sqrt{3}} \right)^{1/2}. \quad (13)$$

The Galton-board model treats transverse dispersion as a mechanistic process [56]. Though it allows to determine D_T using information only about the geometrical structure of the ordered porous medium, diffusion is not considered

as a transport mechanism. Equation (11) predicts that D_T is proportional to the average velocity u and does not depend on the solute diffusion coefficient. This contradicts theoretical findings [54,88,89], experimental data [90,91], and also the results of numerical simulations [14,83,84,92–95]. The Galton-board model assumes that solute molecules in a region of merging flow streamlines experience a complete mixing independent of the time they need to pass this region, i.e., independent of the flow velocity and the diffusion coefficient.

Simpson proposed a modified Galton-board model [57]. It accounts for the dependence of the rate of exchange between solute molecules, brought to a mixing zone through different flow streamlines, on the time that the molecules require to pass the zone. In the Simpson model, the porous medium is represented as an idealized structure of spatially ordered, rectangular cells associated with either solid phase or void space [Fig. 3(a)]. It is assumed that the flow field in the void cells consists of only the uniform longitudinal component determined by the average velocity u through the porous medium. Therefore, the Simpson model does not need to resolve the problem of the actual flow field. Regardless of an eventual discontinuity of the void space in the model resulting from spatially disconnected void cells, time-continuous mass transport is maintained through the assumption of instantaneous lateral displacements of a tracer toward the neighboring downstream void cells as it leaves a given cell [dashed blue lines in Fig. 3]. Each void cell is divided into two halves along the longitudinal x -direction [Fig. 3(b)]. It is assumed that a tracer can enter a downstream void cell only through the fraction of its lateral boundary belonging to the half-cell that is closest to the exited cell. In the absence of diffusion, the tracer leaves a void cell by passing the downstream lateral boundary that belongs to the same half through which it has entered. To account for diffusion as a mixing mechanism in the void cells, Simpson introduced two quantities, q and p ($q + p = 1$), which correspond to the probabilities that a tracer leaves a void cell from the same

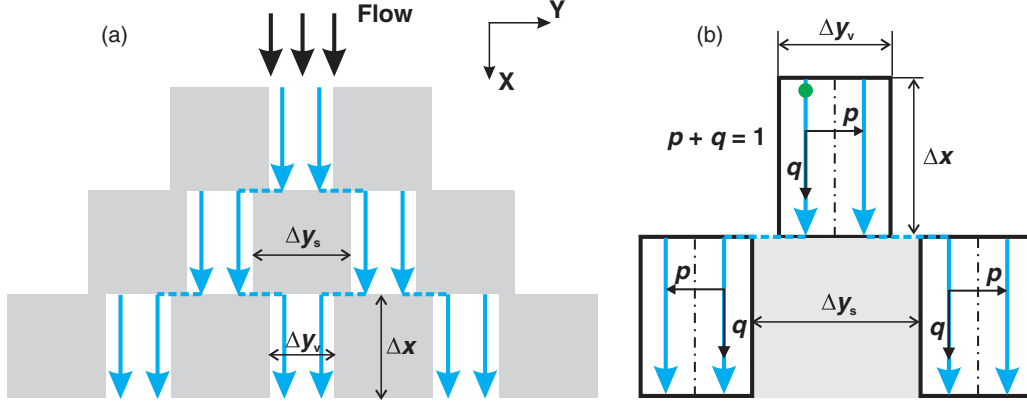


FIG. 3. (a) Idealized representation of a porous medium in the Simpson model. Gray and white rectangular domains represent solid and void cells, respectively. Blue arrows show the uniform flow streamlines in the void cells and the dashed blue lines represent the (instantaneous) lateral displacements of tracers after they leave the void cells. (b) Schematic illustration of diffusive exchange between the two halves of the void cells in the Simpson model. Black dashed-dotted lines indicate the boundaries between the two halves of a void cell. The green filled circle represents a tracer entering with fluid flow a given half of the void cell. After time $\Delta t = u/\Delta x$, the tracer leaves the cell from the same half (with probability q) or through the adjoining half (with probability p).

half through which it has entered and from the adjoining half-cell, respectively. The values of q and p depend on the time Δt that the tracer needs to travel the longitudinal distance Δx (i.e., $\Delta t = \Delta x/u$) and on the diffusion coefficient D_m [cf. Fig. 3(b)].

Simpson proposed to determine the probabilities q and p by resolving a one-dimensional diffusion problem in a rectangular domain divided into two equal halves. Initially, one of the halves contains a uniformly distributed species at concentration c_0 and the second one is empty. Then, the species diffuses through the boundary between the two halves of the domain. Diffusion only normal to the boundary is accounted for. The external boundary of the domain is assumed to be impermeable. The solution of the aforementioned one-dimensional diffusion problem can be obtained as follows [96]:

$$c(y,t) = \frac{c_0}{2} \sum_{j=-\infty}^{\infty} \left[\operatorname{erf} \frac{\frac{\Delta y_v}{2}(1+4j) - y}{2\sqrt{D_m t}} + \operatorname{erf} \frac{\frac{\Delta y_v}{2}(1-4j) + y}{2\sqrt{D_m t}} \right], \quad 0 \leq y \leq \Delta y_v, \quad t \geq 0, \quad (14)$$

where $c(y,t)$ is the species concentration at position y after time t , c_0 is the initial, uniform species concentration in the region $0 \leq y \leq \Delta y_v/2$, and $\Delta y_v = d_p(1-\phi)/2\phi$. The value of p is determined as the fraction of species diffused across the boundary after time Δt . This fraction is calculated by integrating $c(y,t = \Delta t)$ with respect to y over the range $\Delta y_v/2 \leq y \leq \Delta y_v$:

$$p = \frac{2}{c_0 \Delta y_v} \int_{\Delta y_v/2}^{\Delta y_v} c(y,t = \Delta t) dy. \quad (15)$$

With this approach, p does not depend on the initial species concentration; i.e., the calculated value of p is applied to characterize diffusive transport in all void cells independent of their position in the system. Then, the variance of the transverse displacement of the tracer from its original position

after passing n void cells is given by [85]

$$\sigma_{T,n}^2 = \frac{(\Delta y_v + \Delta y_s)^2}{4} np, \quad (16)$$

and the corresponding value of D_T is calculated as

$$D_T = \frac{1}{8} \frac{(\Delta y_v + \Delta y_s)^2}{\Delta x} up, \quad (17)$$

where $\Delta y_s = \Delta y_v/(\phi^{-1} - 1)$. Comparison of Eqs. (11) and (17) shows that the Simpson model is reduced to the Galton-board model when $\Delta y_v = \Delta y_s = \Delta y$ and $p = 0.5$. (It should be noted that Δx in the Simpson model is half the longitudinal dimension of the unit cell in the Galton-board model, cf. Figs. 2 and 3.) The value of $p = 0.5$ corresponds to a complete mixing of tracers during their motion in a void cell, which can be observed if $u \rightarrow 0$ (or more rigorously, if $v \rightarrow 0$).

However, the probability p in the Simpson model is not constant. It is a function of velocity u , diffusion coefficient D_m , and the parameters Δx and Δy_v characterizing the geometry of the system. Substituting Eq. (14) into Eq. (15) and integrating with respect to $\Delta y_v/2 \leq y \leq \Delta y_v$ and $t = \Delta t = \Delta x/u$, one can derive the following expression for p [96]:

$$p = \sqrt{\frac{4D_m \Delta x}{u \Delta y_v^2}} \sum_{j=-\infty}^{\infty} \left\{ \left(\exp \frac{-j^2 u \Delta y_v^2}{D_m \Delta x} \right) - \left[\exp \frac{-(1-2j)^2 u \Delta y_v^2}{4D_m \Delta x} \right] \right\} - \sum_{j=-\infty}^{\infty} \left\{ 2j \operatorname{erfc} \left(\frac{j \sqrt{u \Delta y_v^2}}{\sqrt{D_m \Delta x}} \right) - (1-2j) \operatorname{erfc} \left[\frac{(1-2j) \sqrt{u \Delta y_v^2}}{2\sqrt{D_m \Delta x}} \right] \right\}. \quad (18)$$

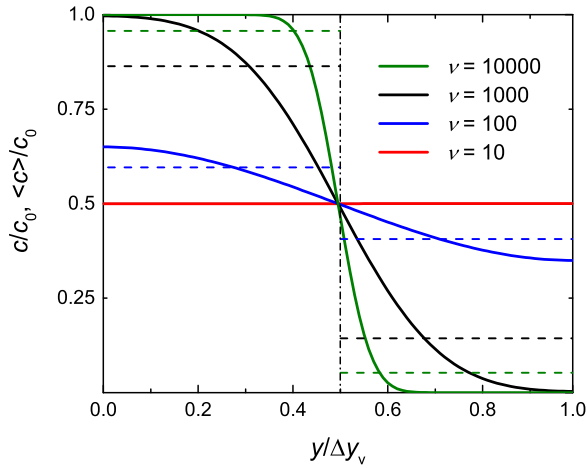


FIG. 4. Normalized lateral concentration distributions c/c_0 (solid lines) of species in a void cell after the time $\Delta t = \Delta x d_p / \nu D_m$, calculated according to Eq. (14), for different reduced velocities ν . Species were initially distributed with uniform concentration ($c/c_0 = 1$) in the region $0 \leq y/\Delta y_v \leq 0.5$. The dashed lines represent normalized average species concentrations ($\langle c \rangle / c_0$) in the left and right halves of the void cell after Δt .

By asymptotic analysis for $u \rightarrow \infty$, the value of p can be approximated as

$$p = \sqrt{\frac{4D_m \Delta x}{u \Delta y_v^2 \pi}}, \quad (19)$$

and after substituting Eq. (19) into Eq. (17), the following functional dependence of D_T on u can be developed:

$$D_T \propto u^{1/2}. \quad (20)$$

Though Eq. (20), in contrast to Eq. (11), predicts a nonlinear dependence of D_T on the flow velocity in a porous medium, the above functional relation with u still contradicts experimental data [60] and the results of numerical simulations [83,92,95], indicating that D_T in ordered porous media approaches an asymptotic value with increasing flow velocity.

Our analysis of the Simpson model has demonstrated that this disagreement originates from the assumption of a uniform species concentration in the void cells that is used as initial condition for resolving the diffusion problem (to determine the value of p). The incorrectness of this assumption is illustrated by the data presented in Fig. 4. The solid lines in this figure show the lateral distribution of the normalized species concentration (c/c_0) in a void cell after different times $\Delta t = \Delta x d_p / \nu D_m$ associated with different reduced velocities ν (Δt is the time available for lateral diffusion of a tracer in a void cell, equal to the length of the cell divided by the flow velocity). The normalized lateral concentration distributions in Fig. 4 were obtained according to Eq. (14) for initially uniform concentration distribution ($c/c_0 = 1$) in the left half of the void cell [$0 \leq y/\Delta y_v \leq 0.5$, Fig. 3(b)]. The results in Fig. 4 demonstrate that for $\nu \geq 100$ the lateral concentration distributions are nonuniform. According to the Simpson model, the nonuniform concentration distribution established in the current void cell after time Δt is replaced by the corresponding uniform one (dashed lines in Fig. 4),

which is used as initial boundary condition for the next two downstream void cells [Fig. 3(b)]. The uniform concentrations are obtained by averaging the concentration distributions in the left and right halves of the current cell. This replacement allows to avoid recalculation of p in every void cell and, consequently, reduces significantly the numerical expenses for the determination of D_T . At the same time, the above probabilistic approach leads to an inaccurate solution for the diffusion problem in the void cells due to the incorrect initial boundary conditions. In the Simpson model the actual concentration distribution established in a void cell after time $\Delta t = \Delta x d_p / \nu D_m$ is replaced by the average concentrations in the left and right halves of the cell. At $\nu \leq 10$, when Δt is sufficiently large, the actual concentration after Δt is almost uniform and can be quite accurately represented by its average value. With increasing ν , Δt becomes smaller and tracers diffuse a shorter average distance. This results in a non-uniform lateral concentration distribution established within the void cell after time Δt . Therefore, the average concentration $\langle c \rangle$ in the right half of the cell becomes higher than the actual concentration at the right side of the cell, $c_R = c(y = \Delta y_v)$. The relative difference $(\langle c \rangle - c_R) / c_R$ increases with ν (because c_R decreases with ν). In turn, at the next iteration, this leads to an increased fraction of tracers that diffuse to the right half of the right downstream void cell, resulting in an overestimation of the mean squared displacement in the Simpson model at high ν .

We modified the Simpson model by introducing a calculation of the concentration distribution in every void cell of the system. For this purpose, the modeled system was represented as large hexagonal array of discs composed of 30,000 layers. Figure 5 shows a section of the array with its first three layers. Similar to the original Simpson model, void cells with dimensions Δx and Δy_v (semi-transparent red rectangular regions in Fig. 5) were used to represent

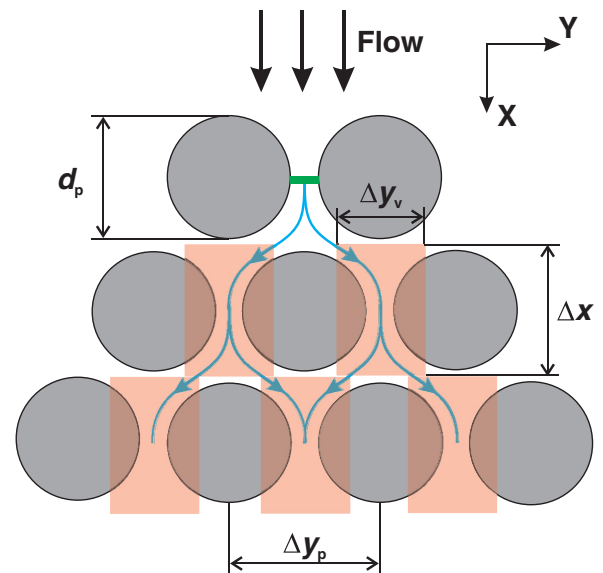


FIG. 5. Simplified representation of the geometrical structure of the hexagonal array. Void cells are shown as (semi-transparent) red rectangular regions. The green horizontal line indicates the position of tracers at $t = 0$.

the void space of the array. At $t = 0$, tracers are placed in the space between two discs of the first layer with uniform concentration c_0 (green horizontal line in Fig. 5). Then, the concentration distribution in every void cell of the system is successively calculated, while accounting for the generally nonuniform initial concentration distribution obtained from solutions for the one-dimensional diffusion problem in two adjoining (upstream) void cells.

A solution for this one-dimensional diffusion problem with initially non-uniform concentration distribution can be obtained by a superposition-reflection method [96]. For this purpose, we divided the void cells along the y -direction into

L equal regions with dimension $\Delta y_v/L$ (here, $L = 100$). The initial (entering) concentration c_{l0} in the l th ($0 < l \leq L$) region was assumed to be uniform and equal to the concentration in the center of the region, $y_l = (l - 0.5)\Delta y_v/L$. Then, a solution for this diffusion problem can be represented as a superposition of solutions for individual subproblems resolved for l instant diffusion sources with initial concentration c_{l0} , the same width $\Delta y_v/L$, and positioned between $(l - 1)\Delta y_v/L$ and $l\Delta y_v/L$. Assuming an impermeability of the external boundary of a void cell, the concentration c_l at the center of the l th region $y_l = (l - 0.5)\Delta y_v/L$ after time $\Delta t = \Delta x \Delta y_v / \nu D_m$ can be calculated according to the following expression:

$$c_l = \frac{1}{2} \sum_{k=1}^L c_{k0} \left\{ \operatorname{erf} \left(\frac{y_l - a_k}{2\sqrt{D_m \Delta t}} \right) + \operatorname{erf} \left(\frac{y_l + b_k}{2\sqrt{D_m \Delta t}} \right) - \operatorname{erf} \left(\frac{y_l + a_k}{2\sqrt{D_m \Delta t}} \right) - \operatorname{erf} \left(\frac{y_l - b_k}{2\sqrt{D_m \Delta t}} \right) \right. \\ \left. + \sum_{j=1}^{\infty} \left[\operatorname{erf} \left(\frac{2j\Delta y_v - y_l - a_k}{2\sqrt{D_m \Delta t}} \right) - \operatorname{erf} \left(\frac{2j\Delta y_v + y_l + a_k}{2\sqrt{D_m \Delta t}} \right) + \operatorname{erf} \left(\frac{2j\Delta y_v - y_l + b_k}{2\sqrt{D_m \Delta t}} \right) \right. \right. \\ \left. \left. - \operatorname{erf} \left(\frac{2j\Delta y_v + y_l - b_k}{2\sqrt{D_m \Delta t}} \right) + \operatorname{erf} \left(\frac{2j\Delta y_v + y_l - a_k}{2\sqrt{D_m \Delta t}} \right) - \operatorname{erf} \left(\frac{2j\Delta y_v - y_l + a_k}{2\sqrt{D_m \Delta t}} \right) \right. \right. \\ \left. \left. + \operatorname{erf} \left(\frac{2j\Delta y_v + y_l + b_k}{2\sqrt{D_m \Delta t}} \right) - \operatorname{erf} \left(\frac{2j\Delta y_v - y_l - b_k}{2\sqrt{D_m \Delta t}} \right) \right] \right\}, \quad (21)$$

where $a_k = (k - 1)\Delta y_v/L$ and $b_k = k\Delta y_v/L$ ($0 < k \leq L$). Thus, Eq. (21) allows us to determine the tracer concentration distribution in the system after time $t + \Delta t$ depending on the concentration distributions in the void cells at time t .

A principle distinction of this approach from the original Simpson model is the elimination of the averaging procedure used to produce uniform tracer concentrations in the two halves of a void cell as initial condition for resolving the local diffusion problem. This modification allows to account for diffusive fluxes originating in lateral concentration gradients in each void cell. In contrast to the original Simpson model, the tracer concentration distribution is determined not only by ν and the geometrical parameters characterizing the structure of the array (Δx , Δy_v , and Δy_p), but also by the position of a void cell in the array. Therefore, D_T cannot be calculated with Eq. (17), because the value of p in the proposed modification of the Simpson model is not the same any more in different void cells of the system. To evaluate the transverse dispersion coefficient obtained with the proposed model, we used the method of moments [17,26,86,87]. According to this method, $D_T(t)$ can be calculated from the variance of the transverse displacement of tracers from their original position (cf. Fig. 5) as

$$D_T(t) = \frac{d\sigma_T^2}{2dt}. \quad (22)$$

Replacing the derivative by its finite-difference approximation, Eq. (22) can be rewritten as

$$D_T(t) = \frac{\sigma_{T,n}^2 - \sigma_{T,n-1}^2}{2\Delta t} = \frac{\Delta\sigma_{T,n}^2}{2\Delta t}, \quad (23)$$

where $\sigma_{T,n}^2$ is the variance of the transverse displacement of tracers after passing n layers of the hexagonal array and $t = n\Delta t$. For a large number of tracers $\sigma_{T,n}^2$ is equivalent to the variance of the transverse concentration distribution of tracers at the n th layer of the array.

The modeling of transverse dispersion, employing the approach described above, is carried out according to the following iterative scheme. At the beginning of each time-iteration with the duration $\Delta t = \Delta x d_p / \nu D_m$, the initial (entering) concentration distribution for every rectangular void cell is spatially associated with the distribution at its upper (upstream) lateral boundary (cf. Fig. 3). Then, Eq. (21) is used to determine the concentration distribution established in a void cell after time Δt through lateral diffusion. This concentration distribution corresponds to that observed at the bottom (downstream) lateral boundary of the void cell, assuming a uniform x -component and zero y -component of flow velocity in the cell. Transverse advective transport in the system is realized by introducing instant lateral displacements of the tracers after time Δt from the bottom (downstream) lateral boundary of a given void cell to the upper boundaries of two adjoining downstream void cells. Since the splitting of flow streamlines enveloping a disc in a hexagonal array is symmetric, the outgoing concentration distribution calculated for a given void cell is also split into two equal halves, left and right (cf. Fig. 3). At the end of an iteration, each of the halves is transferred to the left or right nearest downstream void cells and set as the initial concentration distribution at the next iteration for the right or left halves of the left or right downstream cells, respectively.

In contrast to the Simpson model, the proposed approach requires resolving a diffusion problem for each void cell.

However, it allows to model more realistically diffusive transport resulting from lateral concentration gradients in a porous medium. This transport significantly affects the exchange between species carried by different flow streamlines and, therefore, the transverse dispersion coefficient. In the next two sections, we present results obtained through analyzing the effect of order/disorder (and the finite value of D_m) on D_T in the hexagonal and random arrays of discs using the proposed approach.

IV. HEXAGONAL ARRAY OF DISCS

The system we analyze in this section is a hexagonal array of discs with solid volume fraction $\phi = 0.6$, which is between the limits corresponding to random-loose (~ 0.55) and random-close packing (~ 0.64) for monosized, frictionless hard spheres [97]. Similar to the representation of a porous medium used in the Simpson model, the real geometrical structure of the array is replaced by spatially ordered void cells with longitudinal and transverse dimensions Δx and Δy_v , respectively (cf. Fig. 5). The lateral distance between the centers of two neighboring void cells in the same layer is Δy_p . The values of Δx and Δy_p are determined by the disc diameter and the solid volume fraction in the array

$$\Delta x = \frac{d_p}{2} \left(\frac{\pi \sqrt{3}}{2\phi} \right)^{1/2} \quad (24)$$

and

$$\Delta y_p = d_p \left(\frac{\pi}{2\phi \sqrt{3}} \right)^{1/2}. \quad (25)$$

The lateral dimension Δy_v of the void cells was determined by adjusting the hydraulic diameter of the rectangular void cell to that of the actual pore in the hexagonal array:

$$\Delta y_v = \frac{d_p(1 - \phi)}{2\phi}. \quad (26)$$

At $t = 0$, the tracers are placed in the gap space between two discs of the first layer ($n = 0$) with a uniform concentration. The fluid flow in a void cell has only one constant longitudinal component u . Transverse displacement of tracers from upstream void cells to downstream cells occurs with frequency $1/\Delta t = u/\Delta x$. The length of these displacements is $\Delta y_p/2$. The time-dependent transverse dispersion coefficient $D_T(t)$ was calculated according to Eq. (23) using the variances of the transverse concentration distributions determined at layers n and $(n - 1)$ of the array, where $t = n\Delta t$.

Figure 6 shows how the values of $\Delta\sigma_{T,n}^2/\Delta t$ change with increasing number of passed layers, n , in the hexagonal array at several reduced flow velocities $\nu = ud_p/D_m$. Different values of ν were realized by adjustment of the fluid flow velocity u , assuming $d_p = 10^{-5}$ m and $D_m = 10^{-9}$ m² s⁻¹. The results in Fig. 6 show that the behavior of $\Delta\sigma_{T,n}^2/\Delta t$ at high ν is characterized by oscillations, which decay with the number of layers passed by the tracers. (To achieve a better visualization, the data at $\nu = 1000$ and $10\,000$ for $n < 10$ and $n < 130$, respectively, have been removed.) This specific oscillatory behavior originates in the initially localized distribution of tracer concentration and the spatially periodic structure of

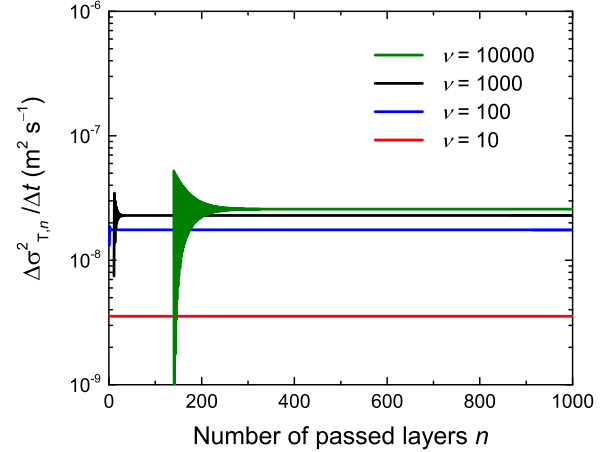


FIG. 6. Dependence of $\Delta\sigma_{T,n}^2/\Delta t$ on the number of passed layers n in a hexagonal disc array with solid volume fraction $\phi = 0.6$ for selected reduced velocities $\nu = ud_p/D_m$. The quantity $\Delta\sigma_{T,n}^2$ is defined as $(\sigma_{T,n}^2 - \sigma_{T,n-1}^2)$, where $\sigma_{T,n}^2$ is the variance of the transverse distribution of the tracer concentration at the n th layer of the array. At the first layer ($n = 0$), tracers were positioned with uniform concentration in the gap space between two discs (cf. Fig. 5). The disc diameter d_p is 10^{-5} m, the free tracer diffusion coefficient D_m is 10^{-9} m² s⁻¹, and $\Delta t = \Delta x/u$. For a better visualization, the data obtained at $\nu = 1000$ and $10\,000$ for $n < 10$ and $n < 130$, respectively, have been removed.

the array. At high ν , the time tracers need to pass a pore with fluid flow is insufficient to equilibrate their concentration by lateral diffusion (cf. Fig. 4). Consequently, the transverse position of tracers after passing the first few layers of the array is mainly governed by splitting and merging of flow streamlines, resulting in abrupt changes in σ_T^2 calculated at two successive layers. With increasing number of passed layers, the variance of the transverse concentration distribution becomes progressively affected by lateral diffusion in void cells. This results in a gradual decrease of the difference between values of σ_T^2 calculated at two successive layers and in a corresponding decay of oscillations with n , as observed in Fig. 6. The rate of the oscillation decay depends on the reduced velocity characterizing the ratio between contributions of advection and diffusion to mass transport: The smaller the value of ν the larger is the effect of diffusion on the variance of the transverse concentration distribution.

The data in Fig. 6 reveal that with increasing number of passed layers, the ratio between $\Delta\sigma_{T,n}^2$ and Δt approaches a time-independent, asymptotic value which depends on ν . Independence of $\Delta\sigma_{T,n}^2/\Delta t$ from time means that transverse dispersion in the disc array can be considered as a diffusion-like process. This conclusion is supported by the data in Fig. 7, where the transverse concentration distributions at $n = 10^4$ are shown, calculated with the presented approach at four selected values of ν . All distributions in Fig. 7 are fitted excellently with a Gaussian, resulting in adjusted coefficients of determination equal to unity [98].

Figure 8 shows the dependencies of the transverse dispersion coefficient normalized by D_m on the reduced velocity, obtained with the presented approach (solid circles), the LBM-RWPT simulations (solid line), and the Simpson model

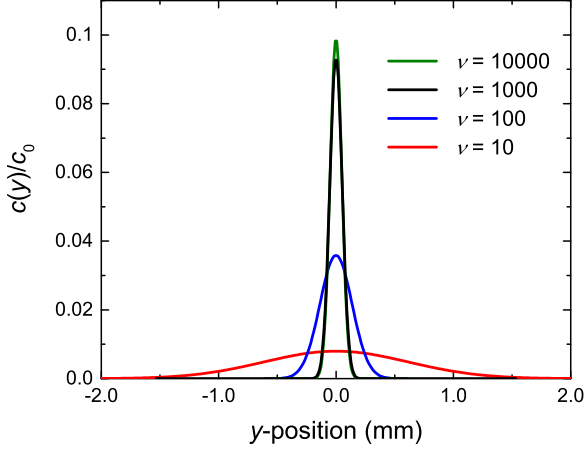


FIG. 7. Normalized transverse tracer concentration distributions $c(y)/c_0$ after passing $n = 10^4$ layers in the hexagonal array of discs with solid volume fraction $\phi = 0.6$ for selected reduced velocities $\nu = ud_p/D_m$. At the first layer ($n = 0$), the tracers were positioned with a uniform concentration $c_0 = 1.0$ in the gap space between two discs (cf. Fig. 5). The diameter of the discs d_p is 10^{-5} m and the free diffusion coefficient of the tracers D_m is 10^{-9} m² s⁻¹.

(open triangles) along with experimental data (open squares) from Ref. [60]. The values of D_T received with the presented approach were calculated according to Eq. (23), using the variances of the transverse tracer concentration distributions determined in the array for $n > 500$, where steady-state (long-time) behavior of $\Delta\sigma_{T,n}^2/\Delta t$ is found (cf. Fig. 6). Though the presented simplified approach does not account for a non-uniform velocity profile in the void space between discs and diffusion in longitudinal direction, it allows not only to reproduce the behavior of D_T/D_m with increasing ν , but also provides D_T -values close to those obtained with a comprehensive simulation approach (LBM–RWPT) and by experimental

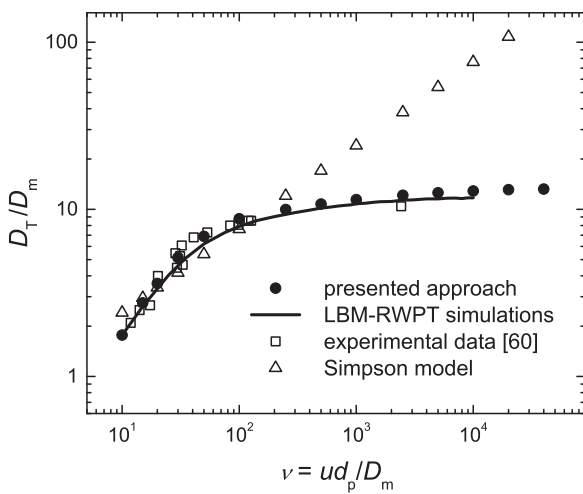


FIG. 8. Dependencies of the normalized transverse dispersion coefficient D_T/D_m on the reduced velocity $\nu = ud_p/D_m$ in a hexagonal disc array with solid volume fraction $\phi = 0.6$, determined according to the presented approach (solid circles), obtained with the LBM–RWPT simulations (solid line), based on the Simpson model (open triangles), and from experiments (open squares) [60].

measurements. By contrast, the original Simpson model is not capable of describing adequately the behavior of D_T at high ν .

The data in Fig. 8 demonstrate that D_T in the studied system for $\nu \geq 10$ exceeds D_m . This confirms that, apart from diffusion, tracer transport in the lateral direction is also realized by an additional mechanism related to advection. During its motion along a flow streamline, a tracer can diffuse to a neighboring streamline. If initial and neighboring streamlines split around the nearest downstream disc (cf. Fig. 5), this results in a change of the transverse tracer position by $\approx \Delta y_p$ after time $\Delta t = \Delta x/2u$ (the time needed by a tracer to pass one half of a layer in the disc array) relative to the transverse position of a tracer that follows the initial streamline. Average diffusive displacement during the same time interval is given by $(2D_m\Delta t)^{1/2} = (2d_p\Delta x/\nu)^{1/2}$ and becomes smaller than Δy_p at high ν . It results in an increased variance of the transverse displacement of tracers (and increased D_T) compared to purely diffusive transport. The above mechanism of enhanced transverse transport can be realized only if $D_m \neq 0$, because with pure advective transport ($D_m = 0$) the tracers always follow their initial flow streamlines. Already a very small diffusive contribution of the tracers (compared to advection) is sufficient to drive the additional advective–diffusive transport mechanism. Thus, realization of the condition $\nu \rightarrow \infty$ following these two diverse approaches ($D_m = 0$ versus $D_m \neq 0$, but $u \rightarrow \infty$) results in a different behavior of D_T in ordered two-dimensional porous systems. While $D_T = 0$ at any value of ν for the purely advective transport, the presence of diffusion leads to an increase of D_T with ν which, however, lessens monotonically.

The difference in the functional dependence of D_T on ν , observed at moderate ($\nu < 10^2$) and very high ($\nu > 10^3$) values of the reduced velocity (cf. Fig. 8), can be explained by the different spatiotemporal conditions behind the concentration equilibration in the void cells resulting from transverse diffusion. If Δt (the time needed by a tracer to pass a void cell due to flow) is large enough to result in a mean diffusive displacement exceeding the width of the void cell, then any initial (i.e., at the entrance of a void cell) and laterally non-uniform concentration distribution relaxes after Δt into a uniform one, which in turn becomes the initial concentration distribution for the next downstream void cells. This concentration equilibration is a consequence of the two external (right and left), impermeable boundaries of the void cells. It explains why the Simpson model, which assumes a uniform initial concentration for one half of any void cell, can describe the D_T – ν dependence sufficiently accurate at moderate values of ν (cf. Fig. 8). Using Eqs. (24) and (26) (determining the dimensions of the void cells in the hexagonal array), one can define the critical value ν_{crit} for which the average transverse diffusive displacement of the tracers $\langle \Delta y \rangle = (2D_m\Delta t)^{1/2} = (2d_p\Delta x/\nu)^{1/2}$ during the time interval Δt is equal to the half-width of the void cell

$$\nu_{\text{crit}} = \left(\frac{\pi\sqrt{3}}{2\phi} \right)^{1/2} \frac{16\phi^2}{(1-\phi)^2}. \quad (27)$$

For $\nu < \nu_{\text{crit}}$, the presence of the two impermeable boundaries in the void cells noticeably affects the concentration distribution after Δt and drives equilibration within any cell.

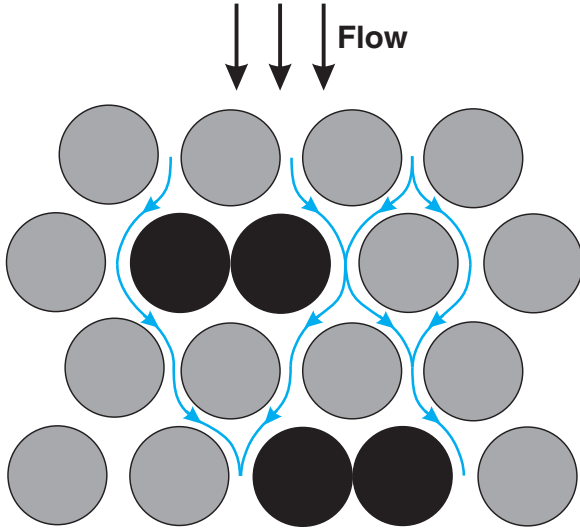


FIG. 9. Region of a structure generated for group *arrays_2*. Black circles correspond to the contacting discs. Such contacting pairs exist in every second layer of the array. In an individual layer, only two randomly chosen discs are allowed to be in contact.

Therefore, ν_{crit} can be considered as the upper limit of the reduced velocity at which the Simpson model still allows to determine D_T with sufficient accuracy. For the hexagonal array of discs with $\phi = 0.6$, Eq. (27) provides $\nu_{\text{crit}} \approx 163$. The data presented in Fig. 8 show that for $\nu < 200$, the Simpson model describes the $D_T - \nu$ dependence in this system satisfactorily.

With a further increase in ν and a corresponding reduction of Δt , the average diffusive displacement of tracers $\langle \Delta y \rangle$ becomes smaller than the half-width of the void cells. For instance, $\langle \Delta y \rangle \approx 0.14 \Delta y_v$ and $0.04 \Delta y_v$ for $\nu = 10^3$ and 10^4 , respectively. This means that the effect of the impermeable walls on the concentration redistribution (equilibration) within the void cells during Δt decreases with ν . At very high values of ν , only tracers located initially (at the entrance of the void cells) very closely to the boundary between the right and left halves of a void cell can cross this boundary during Δt and subsequently change their transverse position

by Δy_p . Therefore, the mechanism for transverse dispersion becomes dominated by successive changes in the tracers' transverse positions, resulting from the exchange between the two halves of the void cells. The probability of this exchange is proportional to Δt and inversely proportional to the average flow velocity and ν . On the other hand, the number of the void cells that a tracer visits per time is proportional ν . This causes D_T to approach a constant value at high values of ν .

In the next section, we present results obtained with the proposed modification of the Simpson model to analyze the effect of diffusion on the transverse dispersion coefficient in disordered two-dimensional porous media.

V. DISORDERED ARRAYS OF DISCS

For this investigation, disordered two-dimensional porous media were generated by disturbing (in a random manner) the geometrical order of the hexagonal array of discs. The distortion was introduced by creating pairs of contacting discs in the layers of the array. In a single layer, only two randomly chosen discs were allowed to touch. To receive a set of porous structures with a graded degree of heterogeneity (DoH), we prepared three classes of disc arrays (all with a solid volume fraction of $\phi = 0.6$), for which single pairs of contacting discs were repeatedly formed in every second, fourth, or tenth layer. Below, we refer to these groups of disordered structures as *arrays_2*, *arrays_4*, and *arrays_10*, respectively. For each group, ten disordered arrays with different positions of the contacting discs were generated. An example of a structure of an array for group *arrays_2* is shown in Fig. 9. The DoH increases with the number of layers containing contacting discs, i.e., $\text{DoH}(\text{arrays}_2) > \text{DoH}(\text{arrays}_4) > \text{DoH}(\text{arrays}_{10}) > \text{DoH}(\text{hexagonal array})$. Then, the evolution of tracers, initially distributed with uniform concentration c_0 in the gap space between two central discs in the first layer of the arrays, was calculated according to Eq. (21). The lateral dimension of the void cells corresponding to the contacting discs was set to zero ($\Delta y_v = 0$).

Figure 10 shows the lateral concentration distributions of tracers after passing $n = 10^4$ layers in two selected

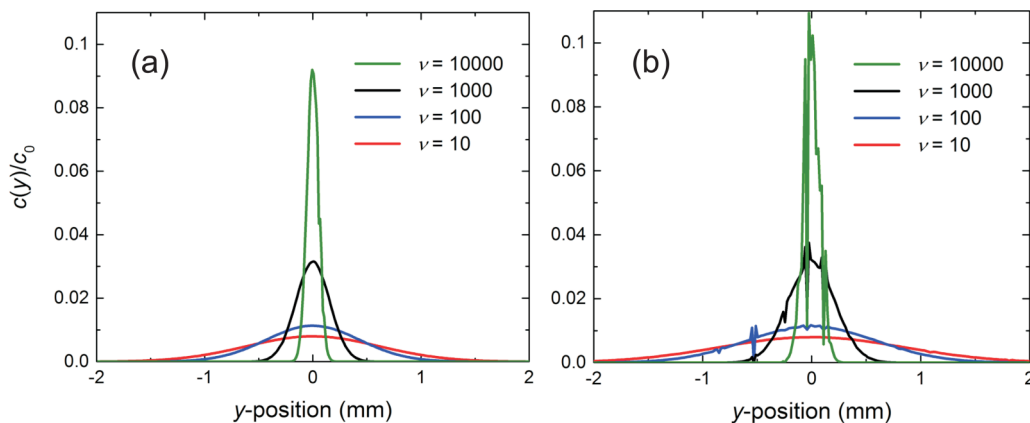


FIG. 10. Normalized transverse concentration distributions of tracers, $c(y)/c_0$, after passing $n = 10^4$ layers in two disordered arrays of discs from groups *arrays_10* (a) and *arrays_2* (b) at selected values of the reduced velocity $\nu = ud_p/D_m$. The solid volume fraction ϕ is 0.6 in both arrays. At the first layer ($n = 0$), the tracers were positioned with a uniform concentration $c_0 = 1.0$ in the gap space between two discs (cf. Fig. 5). The diameter of the discs d_p is 10^{-5} m and the free diffusion coefficient of the tracers D_m is 10^{-9} m² s⁻¹.

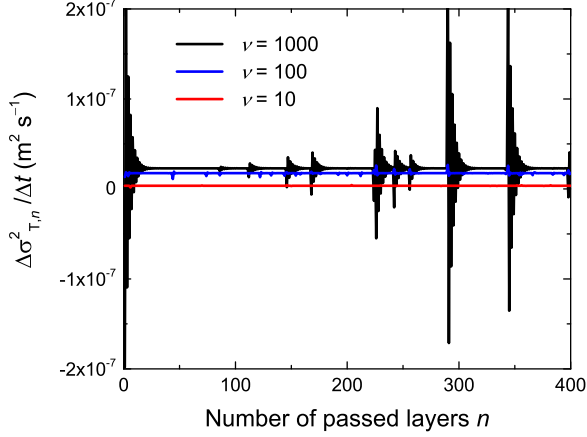


FIG. 11. Dependence of $\Delta\sigma_{T,n}^2/\Delta t$ on the number of passed layers n in a selected disordered structure from group *arrays_2* with solid volume fraction $\phi = 0.6$ at selected reduced velocities $\nu = ud_p/D_m$. The quantity $\Delta\sigma_{T,n}^2$ is defined as $(\sigma_{T,n}^2 - \sigma_{T,n-1}^2)$, where $\sigma_{T,n}^2$ is the variance of the transverse distribution of the tracer concentration at the n th layer of the array. At the first layer ($n = 0$), tracers were positioned with a uniform concentration in the gap space between two discs (cf. Fig. 5). The disc diameter d_p is 10^{-5} m, the free tracer diffusion coefficient D_m is 10^{-9} m² s⁻¹, and $\Delta t = \Delta x/u$.

arrays from groups *arrays_2* and *arrays_10*, obtained at four reduced velocities. Concentration distributions simulated for a random structure from group *arrays_10*, shown in Fig. 10(a), are smooth except for $\nu = 10^4$. By contrast, distributions calculated for a structure from group *arrays_2* [Fig. 10(b)] are characterized by abrupt changes in tracer concentration already at $\nu = 10$. These changes occur at a lateral distance comparable with the disc diameter, implying that their appearance originates in the presence of the disc contacts. Contacting discs in a layer of the array do not allow tracers to be located in the space between these discs after they have been transported from the upstream layer. It results in zero tracer concentration at the transverse position corresponding to the contact point between two discs. During the transport to the next downstream layer of the array, the absence of tracers at some transverse position is partially compensated by advection (represented in the model by lateral

displacements of the tracers between two neighboring layers of the structure) and lateral diffusion in the void cells. However, the relative contribution of diffusion to equilibration of local concentration decreases with higher ν . At low values ($\nu \leq 10$), the time tracers spend to pass a void cell in longitudinal direction is sufficient to achieve a close-to-uniform transverse concentration even in a single void cell (cf. Fig. 4). With increasing ν , this time shortens and local equilibration requires to pass a larger number of void cells. For structures from group *arrays_10*, only every tenth layer contains a pair of contacting discs. Consequently, tracers passing the other nine layers of the array at $\nu \leq 10^3$ have sufficient time for lateral equilibration before experiencing a distortion at the tenth layer. It results in the smooth transverse tracer distributions simulated at $\nu \leq 10^3$, as shown in Fig. 10(a). By contrast, the structures belonging to group *arrays_2* contain contacting pairs of discs in every second layer (Fig. 9). Even at $\nu = 100$, the time that the tracers spend to pass one layer is insufficient for lateral equilibration (cf. Fig. 4). This produces the nonsmooth concentration distributions simulated for $\nu \geq 100$ [Fig. 10(b)].

The presence of the contacting discs is also responsible for the appearance of fluctuations in the dependencies of $\Delta\sigma_{T,n}^2/\Delta t$ on the number of layers that the tracers have passed with the flow. In Fig. 11, we illustrate these dependencies at $\nu = 10, 100$, and 1000 for a selected disordered structure from group *arrays_2*. Random fluctuations in $\Delta\sigma_{T,n}^2/\Delta t$ (observed in Fig. 11) make an evaluation of D_T with Eq. (23) challenging. The determination of the transverse dispersion coefficient according to Eq. (23) is based on the so-called tangent definition of D_T [26]. As an alternative, D_T can be calculated using its secant definition [26]

$$D_T(t) = \frac{\sigma_T^2(t)}{2t}, \quad (28)$$

where $t = n\Delta t$ and n is the number of layers the tracers have passed after time t . According to Eq. (28), the transverse dispersion coefficient can be determined from the slope of σ_T^2 plotted versus time. Figure 12 illustrates this dependence for disordered structures from groups *arrays_10* and *arrays_2* at different ν -values. The functions $\sigma_T^2(t)$ obtained for each of the ten disordered structures from groups *arrays_2*, *arrays_4*, and *arrays_10* were fitted with straight lines and

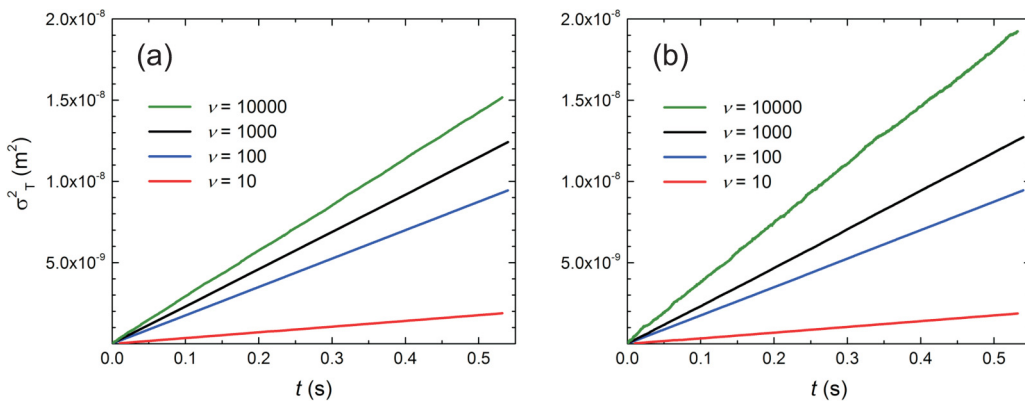


FIG. 12. Variances σ_T^2 of the transverse tracer concentration distributions as a function of time, simulated for two disordered arrays of discs from groups *arrays_10* (a) and *arrays_2* (b) with solid volume fraction $\phi = 0.6$ at selected reduced velocities $\nu = ud_p/D_m$. The diameter of the discs d_p is 10^{-5} m and the free diffusion coefficient of the tracers D_m is 10^{-9} m² s⁻¹.

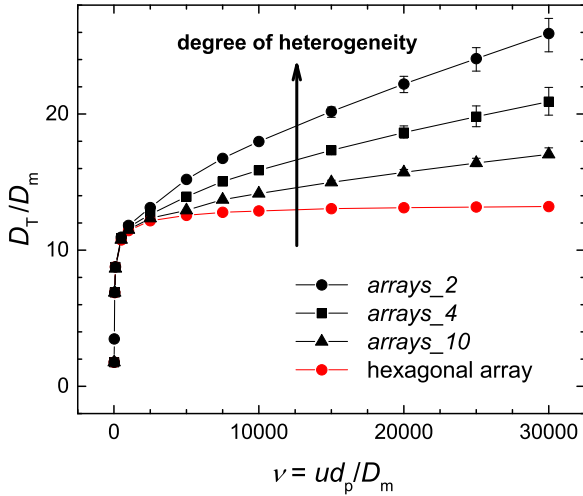


FIG. 13. Normalized transverse dispersion coefficient D_T/D_m vs. the reduced flow velocity $\nu = u d_p / D_m$, determined for the disordered structures (black symbols) and the hexagonal array of discs (red symbols). The solid volume fraction is 0.6, the diameter of the discs d_p is 10^{-5} m, and the free tracer diffusion coefficient D_m is 10^{-9} m² s⁻¹. Black symbols represent the values of D_T/D_m averaged over the ten different realizations for each array group, and the error bars denote the corresponding ranges for the simulated values.

the corresponding transverse dispersion coefficients were determined using Eq. (28). It should be pointed out that the relative difference between D_T -values obtained for the hexagonal array of discs according to Eqs. (23) and (28) did not exceed 2% within the whole range of reduced velocities we analyzed in this study ($10 \leq \nu \leq 4 \times 10^4$).

Figure 13 shows the transverse dispersion coefficient normalized by D_m as a function of the reduced velocity for the three groups of disordered structures (black symbols), determined after Eq. (28), and for the hexagonal array (red circles). Black symbols represent D_T/D_m -values averaged over all ten different realizations for each array group and the error bars indicate the corresponding ranges for the simulated values. Transverse dispersion coefficients determined for the hexagonal array and the disordered structures demonstrate similar values at a given ν in the range $10 \leq \nu \leq 10^3$, but they exhibit a fundamentally different behavior for higher ν . In the hexagonal array, D_T/D_m approaches its asymptotic value of ~ 13.4 , but it increases with ν for the disordered structures: at $\nu \geq 10^4$, the dependence of D_T/D_m on ν becomes close to linear for all disordered arrays of discs. This finding agrees with the simulations by Van Milligen and Bons for an irregular two-dimensional network of channels [36]. Similar to the approach in this study, the model employed by Van Milligen and Bons does not account for Taylor dispersion, i.e., a uniform flow velocity within an individual channel (or a void cell in the present study) is assumed. By contrast, the results in Fig. 1 were obtained by the LBM–RWPT approach, which models advective–diffusive transport with full resolution of the flow field, thereby accounting for the fundamental non-uniformity of the flow velocity at the pore scale. The results obtained with that comprehensive approach for the dependence of D_T/D_m on ν in a structure with a completely random disc arrangement

also reveal the absence of a tapering-off in the dispersion data and the attainment of a plateau with increasing ν (cf. Fig. 1). This allows to conclude that the increase in D_T/D_m with ν , as observed in Figs. 1 and 13 for the disordered structures, does not originate in a non-uniformity of the local flow velocity, but is a result of the random (disordered) geometry of the employed systems.

As mentioned above, the DoH for a disc array increases with the number of layers containing contacting discs (disordered layers). Figure 13 demonstrates a clear relationship between the DoH and slope characterizing the dependence of D_T/D_m on ν for $\nu \geq 10^4$. This dependence becomes steeper with increasing number of disordered layers in a structure. The hexagonal disc array is perfectly ordered and the dependence of D_T/D_m on ν in Fig. 13 is characterized by zero slope (a constant value of D_T/D_m) at high ν . Structures from group *arrays_2* contain pairs of contacting discs in every second layer. It results in the highest DoH among all analyzed structures. The slope of the corresponding dependence of D_T/D_m on ν is steepest compared to the other disc arrays. The observations based on Fig. 13 imply that the geometrical disorder not only changes the behavior of the transverse dispersion coefficient at high reduced velocities (linear dependence of D_T on ν for disordered structures vs. a constant D_T -value for ordered structures), but also determines how strong D_T increases with ν .

Though geometrical disorder is prerequisite to the absence of D_T approaching an asymptotic value at high reduced velocities, this is not a sufficient condition. For purely advective transport ($D_m = 0$), tracers are carried only by the flow along individual streamlines. As a consequence, tracers initially located at the same position keep identical positions also during their transport through a porous medium, independent of a regular or random flow pattern. That scenario can be conceptually realized by allowing the tracers to follow individual streamlines (schematically shown in Figs. 5 and 9), assuming that the exchange between two streamlines is impossible. It results in zero transverse dispersion in both ordered (Fig. 5) and disordered (Fig. 9) structures. This agrees with theoretical results for purely advective transport in two-dimensional porous media [53]. The presence of diffusion changes drastically the behavior of D_T at high reduced velocities. Even an infinitesimal but finite contribution of diffusion (realized at $\nu \rightarrow \infty$) to the exchange of tracers carried with different streamlines results in a non-zero transverse dispersion coefficient in both ordered and disordered two-dimensional structures. If $D_m \neq 0$, there always is a non-zero fraction of tracers that can diffuse from one streamline to another during a finite time interval. Then, the subsequent diverging of the flow streamlines leads to lateral spreading of tracers and a nonzero transverse dispersion coefficient. This scenario is similarly realized in ordered and disordered structures except for one distinction: Regions of splitting and merging of flow streamlines in ordered structures are spatially regular, whereas in disordered structures, they are located at random positions. As a consequence, the lateral position of a tracer carried only by flow in an ordered structure is characterized by time-periodic oscillations with constant amplitude determined only by the characteristic length of the structure (the disc diameter in this study). In a disordered structure, it appears

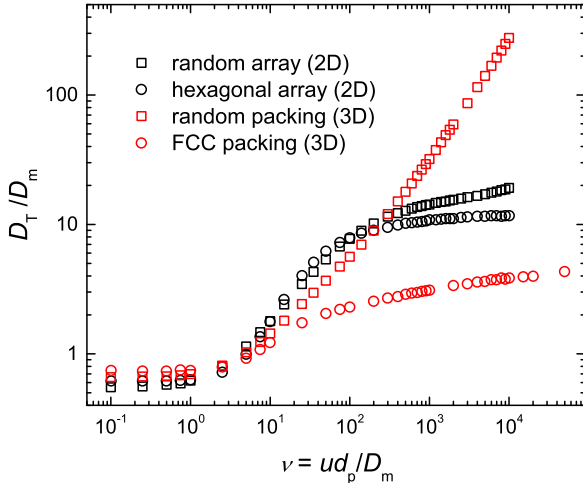


FIG. 14. Transverse dispersion coefficient D_T normalized by the free diffusion coefficient D_m as a function of the reduced velocity $\nu = ud_p/D_m$, obtained by the LBM–RWPT approach, for a hexagonal and a random array of equal discs (black circles and black squares, respectively), and for a FCC and a random packing of equal spheres (red circles and red squares, respectively). The solid volume fraction of all structures is $\phi = 0.6$.

as oscillations with random amplitudes determined also by the length scale characterizing the disorder (the distribution of positions of contacting discs in this study). In combination with diffusion leading to the exchange between neighboring streamlines, this results in completely different behaviors of D_T in ordered and random porous media, as observed at high values of ν (Fig. 13).

Finally, we want to discuss the difference in the dependence of D_T on ν in two- and three-dimensional porous media. Figure 14 shows the normalized transverse dispersion coefficient as a function of ν , obtained with the LBM–RWPT approach, for a hexagonal and a random array of equal discs (black circles and black squares, respectively), and for a FCC (face-centered cubic) and a random packing of monosized spheres (red circles and red squares, respectively). Though all structures have identical solid volume fraction ($\phi = 0.6$), the presented D_T – ν dependencies differ both quantitatively and qualitatively. Similar to the random array of discs, the random packing of spheres is characterized by a linear growth of D_T at high values of the reduced velocity. However, the slope of this growth is larger than for the two-dimensional random structure. It results in much higher values of D_T in the sphere packing than in the random array of discs for $\nu > 10^3$. At the same time, in the range of ν between 10 and 100, the transverse dispersion coefficient in the ordered and random two-dimensional structures is larger than in the random packing of spheres. In contrast to the random structures, the values of D_T in the three-dimensional ordered (FCC) structure at high ν are significantly smaller than in the two-dimensional ordered system. Moreover, D_T in the FCC packing of spheres does not tend to flatten even at $\nu = 5 \times 10^4$. The data in Fig. 14 demonstrate that results and conclusions on transverse dispersion in two-dimensional porous media cannot be straightforwardly applied to three-dimensional media.

VI. CONCLUSIONS

The goal of this study was an investigation into the effect of order and disorder in two-dimensional porous media on the transverse dispersion coefficient (D_T) and its behavior in dependence of the reduced velocity (ν), characterizing the ratio between advective and diffusive contributions to mass transfer. Advective–diffusive transport has been simulated in hexagonal and disordered arrays of equal discs. While the hexagonal array represents an ordered porous medium, the disordered arrays mimic random porous media. Disorder has been realized with a distortion of the hexagonal array by the introduction of contacting discs at random positions in its layers. To simulate advective–diffusive transport, an approach based on geometrical representations of the analyzed structures by void and solid cells has been used. Additional physical assumptions of the employed approach involved a uniform flow field in the void cells, diffusion only normal to the flow (i.e., in the transverse direction), and instant lateral transport between the upstream and downstream neighboring void cells. The aforementioned simplifications have been introduced to the model with the only aim to reveal the extent to which order and disorder of a porous medium impacts the dependence of D_T on ν . For this purpose, we have also provided results obtained with a LBM–RWPT approach (Fig. 1), which does not involve these geometrical and physical simplifications. This comprehensive simulation approach is based on a pore-scale simulation of the complete flow field computed for the actual geometry of a porous medium and accounts for diffusion along all directions.

Results obtained with both the LBM–RWPT approach and the proposed simplified model of advective–diffusive transport (Figs. 1 and 13) have revealed that D_T levels off with increasing ν in the ordered porous medium, while it grows linearly in the disordered structures at high ν . Considering the simplifications introduced (intentionally) to the proposed model, this supports the categorical conclusion that the observed distinction in these functional behaviors originates exclusively in the geometrical disorder of the two-dimensional random porous media.

At the same time, realizing this scenario with a zero-diffusion coefficient results in $D_T = 0$ for both ordered and random two-dimensional porous media [53]. Consequently, it is important to distinguish very clearly between the two possible (and different) cases to achieve the condition $\nu \rightarrow \infty$. The first one ($D_m = 0$) is unphysical and realized at any velocity. In this case, tracers strictly follow the individual flow streamlines during their transport through a porous medium. This results in a zero-transverse dispersion coefficient in ordered and random structures at any value of the flow velocity, u . The second case is realized as u approaches infinity, but $D_m \neq 0$. Then, an increase in the flow velocity has a two-fold effect: It reduces the time for diffusive exchange between neighboring streamlines and increases the number of exchange regions (that a tracer visits per time) proportionally to the value of u . Depending on the geometrical structure and corresponding pattern of the flow field, this results at high values of ν in either a constant value of D_T (ordered porous media) or a linear growth of D_T with ν (random porous media). Figure 13 shows that the slope characterizing this growth depends on the DoH of a structure. The slope is zero for the hexagonal disc array and

increases with the number of the introduced structural defects (contacting discs).

It should be noted that the morphological descriptor based on the number of contacting discs cannot be applied to random arrays, because their heterogeneity does not originate in the (systematically and exclusively) introduced pairs of contacting discs. Therefore, the derivation of relationships between the transverse dispersion coefficient and parameters characterizing the geometrical structure of a porous medium requires the identification of alternative, universal morphological descriptors. This identification is still an outstanding scientific problem. One of the promising approaches is based on using spatial tessellations of the void space in porous media. For instance, it was shown that the second and third statistical moments of the volume distributions for the Voronoi cells in computer-generated random packings of monosized spherical particles and the longitudinal dispersion coefficients

(D_L) show a highly similar dependence on the solid volume fraction and packing protocol (resulting in different packing microstructures) [99]. However, the quantitative incorporation of information obtained with the statistical analysis of the Voronoi volume distributions into morphology–transport relationships is a still unresolved problem.

ACKNOWLEDGMENTS

This work was supported by the Deutsche Forschungsgemeinschaft DFG (Bonn, Germany) under Grant No. TA 268/9–1. Computational resources on IBM BlueGene/Q systems were provided by Forschungszentrum Jülich (FZJ, Jülich, Germany). We thank the John von Neumann Institute for Computing (NIC) and the Jülich Supercomputing Center (JSC) at FZJ for the allocation of a special CPU-time grant (NIC Project No. 10214, JSC Project ID: HMR10).

-
- [1] F. A. L. Dullien, *Porous Media: Fluid Transport and Pore Structure* (Academic Press, San Diego, 1992).
- [2] D. A. Nield and A. Bejan, *Convection in Porous Media* (Springer, New York, 1999).
- [3] S. Torquato, *Random Heterogeneous Materials: Microstructure and Macroscopic Properties* (Springer, New York, 2002).
- [4] M. Sahimi, *Heterogeneous Materials: Vol. I. Linear Transport and Optical Properties* (Springer, New York, 2003).
- [5] M. Sahimi, *Flow and Transport in Porous Media and Fractured Rock: From Classical Methods to Modern Approaches* (Wiley-VCH, Weinheim, 2011).
- [6] J. Bear, *Dynamics of Fluids in Porous Media* (Elsevier, New York, 1972).
- [7] U. M. Scheven, *Phys. Rev. Lett.* **110**, 214504 (2013).
- [8] H. Brenner, *Philos. Trans. R. Soc. London A* **297**, 81 (1980).
- [9] J. Salles, J.-F. Thovert, R. Delannay, L. Prevors, J.-L. Auriault, and P. M. Adler, *Phys. Fluids A* **5**, 2348 (1993).
- [10] S. Whitaker, *Chem. Eng. Sci.* **21**, 291 (1966); *AIChE J.* **13**, 420 (1967).
- [11] W. G. Gray, *Chem. Eng. Sci.* **30**, 229 (1975).
- [12] R. G. Carbonell and S. Whitaker, *Chem. Eng. Sci.* **38**, 1795 (1983).
- [13] M. Quintard and S. Whitaker, *Chem. Eng. Sci.* **48**, 2537 (1993).
- [14] H. P. Amaral Souto and C. Moyne, *Phys. Fluids* **9**, 2253 (1997).
- [15] D. L. Koch and J. F. Brady, *J. Fluid Mech.* **154**, 399 (1985).
- [16] B. P. van Milligen and P. D. Bons, *Phys. Rev. E* **85**, 011306 (2012).
- [17] G. De Josselin De Jong, *Trans. Am. Geophys. Union* **39**, 67 (1958).
- [18] P. G. Saffman, *J. Fluid Mech.* **6**, 321 (1959); **7**, 194 (1960).
- [19] R. A. Greenkorn and D. P. Kessler, *Ind. Eng. Chem.* **61**, 14 (1969).
- [20] R. E. Haring and R. A. Greenkorn, *AIChE J.* **16**, 477 (1970).
- [21] L. Torelli, *Pure Appl. Geophys.* **96**, 75 (1972).
- [22] S. Mandel and Z. Weinberger, *J. Hydrol.* **16**, 147 (1972).
- [23] M. Sahimi and A. O. Imdakm, *J. Phys. A* **21**, 3833 (1988).
- [24] C. Bruderer and Y. Bernabé, *Water Resour. Res.* **37**, 897 (2001).
- [25] O. Huseby, J.-F. Thovert, and P. M. Adler, *Phys. Fluids* **13**, 594 (2001).
- [26] L. M. Bryntesson, *J. Chromatogr. A* **945**, 103 (2002).
- [27] B. Bijeljic, A. H. Muggeridge, and M. J. Blunt, *Water Resour. Res.* **40**, 11501 (2004).
- [28] R. C. Acharya, S. E. A. T. M. Van der Zee, and A. Leijnse, *Water Resour. Res.* **41**, W02020 (2005).
- [29] L. Li, C. A. Peters, and M. A. Celia, *Adv. Water Resour.* **29**, 1351 (2006).
- [30] B. Bijeljic and M. J. Blunt, *Water Resour. Res.* **42**, W01202 (2006); **43**, W12S11 (2007).
- [31] R. C. Acharya, M. I. J. Van Dijke, K. S. Sorbie, S. E. A. T. M. Van der Zee, and A. Leijnse, *Adv. Water Resour.* **30**, 199 (2007).
- [32] R. C. Acharya, S. E. A. T. M. Van der Zee, and A. Leijnse, *Adv. Water Resour.* **30**, 261 (2007).
- [33] C. Varloteaux, M. T. Vu, S. Békri, and P. M. Adler, *Phys. Rev E* **87**, 023010 (2013).
- [34] J. P. Noguees, J. P. Fitts, M. A. Celia, and C. A. Peters, *Water Resour. Res.* **49**, 6006 (2013).
- [35] Y. Mehmani, M. Oostrom, and M. T. Balhoff, *Water Resour. Res.* **50**, 2488 (2014).
- [36] B. P. Van Milligen and P. D. Bons, *Comput. Phys. Commun.* **185**, 3291 (2014).
- [37] P. K. Kang, M. Dentz, T. Le Borgne, and R. Juanes, *Phys. Rev. E* **92**, 022148 (2015).
- [38] P. Spanne, J.-F. Thovert, C. J. Jacquin, W. B. Lindquist, K. W. Jones, and P. M. Adler, *Phys. Rev. Lett.* **73**, 2001 (1994).
- [39] D. Coelho, J.-F. Thovert, and P. M. Adler, *Phys. Rev. E* **55**, 1959 (1997).
- [40] B. Manz, L. F. Gladden, and P. B. Warren, *AIChE J.* **45**, 1845 (1999).
- [41] R. Gonzalez-Garcia, O. Huseby, J.-F. Thovert, and P. M. Adler, *J. Geophys. Res. B* **105**, 21387 (2000).
- [42] S. Békri and P. M. Adler, *Int. J. Multiphase Flow* **28**, 665 (2002).
- [43] D. Hlushkou, S. Bruns, and U. Tallarek, *J. Chromatogr. A* **1217**, 3674 (2010).
- [44] D. Hlushkou, S. Bruns, A. Höltsel, and U. Tallarek, *Anal. Chem.* **82**, 7150 (2010).
- [45] D. Hlushkou, S. Bruns, A. Seidel-Morgenstern, and U. Tallarek, *J. Sep. Sci.* **34**, 2026 (2011).

- [46] H. Koku, R. S. Maier, K. J. Czymmek, M. R. Schure, and A. M. Lenhoff, *J. Chromatogr. A* **1218**, 3466 (2011).
- [47] H. Koku, R. S. Maier, M. R. Schure, and A. M. Lenhoff, *J. Chromatogr. A* **1237**, 55 (2012).
- [48] P. Mostaghimi, B. Bijeljic, and M. J. Blunt, *SPE J.* **17**, 1131 (2012).
- [49] M. J. Blunt, B. Bijeljic, H. Dong, O. Gharbi, S. Iglauer, P. Mostaghimi, A. Paluszny, and C. Pentland, *Adv. Water Resour.* **51**, 197 (2013).
- [50] B. Bijeljic, A. Raicini, P. Mostaghimi, and M. J. Blunt, *Phys. Rev. E* **87**, 013011 (2013).
- [51] P. K. Kang, P. De Anna, J. P. Nunes, B. Bijeljic, M. J. Blunt, and R. Juanes, *Geophys. Res. Lett.* **41**, 6184 (2014).
- [52] D. R. Steward, *Water Resour. Res.* **34**, 1345 (1998).
- [53] S. Attinger, M. Dentz, and W. Kinzelbach, *Stoch. Environ. Res. Risk Assess.* **18**, 9 (2004).
- [54] D. L. Koch, R. G. Cox, H. Brenner, and J. F. Brady, *J. Fluid Mech.* **200**, 173 (1989).
- [55] W. S. Jodrey and E. M. Tory, *Phys. Rev. A* **32**, 2347 (1985).
- [56] S. T. Sie and G. W. A. Rijnders, *Anal. Chim. Acta* **38**, 3 (1967).
- [57] E. S. Simpson, *Transverse Dispersion in Liquid Flow Through Porous Media: Geological Survey Professional Paper 411-C* (United States Government Printing Office, Washington, 1962).
- [58] M. A. Theodoropoulou, V. Karpusos, C. Kaspiris, and C. D. Tsakiroglou, *J. Hydrol.* **274**, 176 (2003).
- [59] P. Gaganis, E. D. Skouras, M. A. Theodoropoulou, C. D. Tsakiroglou, and V. N. Burganos, *J. Hydrol.* **307**, 79 (2005).
- [60] S. De Bruyne, W. De Malsche, S. Deridder, H. Gardeniers, and G. Desmet, *Anal. Chem.* **86**, 2947 (2014).
- [61] K. N. Smirnov and O. A. Shpigun, *J. Chromatogr. A* **1375**, 27 (2015).
- [62] J. P. Grinias and R. T. Kennedy, *Trends Anal. Chem.* **81**, 110 (2016).
- [63] S. Succi, *The Lattice Boltzmann Equation: For Fluid Dynamics and Beyond* (Oxford University Press, New York, 2001).
- [64] S. Chen and G. D. Doolen, *Annu. Rev. Fluid Mech.* **30**, 329 (1998).
- [65] S. Chapman and T. G. Cowling, *The Mathematical Theory of Non-Uniform Gases*, 2nd ed. (Cambridge University Press, Cambridge, 1952).
- [66] Y. H. Qian, D. d'Humières, and P. Lallemand, *Europhys. Lett.* **17**, 479 (1992).
- [67] D. H. Rothman and S. Zaleski, *Lattice-Gas Cellular Automata* (Cambridge University Press, Cambridge, 1987).
- [68] X. He and L.-S. Luo, *J. Stat. Phys.* **88**, 927 (1997).
- [69] M. A. Gallivan, D. R. Noble, J. G. Georgiadis, and R. O. Buckius, *Int. J. Numer. Meth. Fluids* **25**, 249 (1997).
- [70] D. Hlushkou, K. Hormann, A. Höltzel, S. Khirevich, A. Seidel-Morgenstern, and U. Tallarek, *J. Chromatogr. A* **1303**, 28 (2013).
- [71] S. Khirevich, A. Höltzel, and U. Tallarek, *Commun. Comput. Phys.* **13**, 801 (2013).
- [72] A. F. B. Tompson, E. G. Vomvoris, and L. W. Gelhar, Numerical Simulation of Solute Transport in Randomly Heterogeneous Porous Media: Motivation, Model Development and Application, Technical Report 316 Ralph M. Parsons Laboratory, Massachusetts Institute of Technology, 1988.
- [73] P. Szymczak and A. J. C. Ladd, *Phys. Rev. E* **68**, 036704 (2003).
- [74] R. S. Maier, D. M. Kroll, R. S. Bernard, S. E. Howington, J. F. Peters, and H. T. Davis, *Phys. Fluids* **12**, 2065 (2000); **15**, 3795 (2003).
- [75] D. Kandhai, D. Hlushkou, A. G. Hoekstra, P. M. A. Sloot, H. Van As, and U. Tallarek, *Phys. Rev. Lett.* **88**, 234501 (2002).
- [76] D. Kandhai, U. Tallarek, D. Hlushkou, A. Hoekstra, P. M. A. Sloot, and H. Van As, *Philos. Trans. R. Soc. Lond. A* **360**, 521 (2002); R. S. Maier, D. M. Kroll, R. S. Bernard, S. E. Howington, J. F. Peters, and H. T. Davis, *ibid.* **360**, 497 (2002).
- [77] M. R. Schure, R. S. Maier, D. M. Kroll, and H. T. Davis, *J. Chromatogr. A* **1031**, 79 (2004).
- [78] F. J. Jiménez-Hornero, J. V. Giráldez, and A. Laguna, *Vadose Zone J.* **4**, 310 (2005).
- [79] H. Freund, J. Bauer, T. Zeiser, and G. Emig, *Ind. Eng. Chem. Res.* **44**, 6423 (2005).
- [80] S. Khirevich, A. Höltzel, D. Hlushkou, and U. Tallarek, *Anal. Chem.* **79**, 9340 (2007).
- [81] A. Daneyko, S. Khirevich, A. Höltzel, A. Seidel-Morgenstern, and U. Tallarek, *J. Chromatogr. A* **1218**, 8231 (2011).
- [82] T. R. Brosten, S. L. Codd, R. S. Maier, and J. D. Seymour, *Phys. Fluids* **23**, 093105 (2011).
- [83] A. Daneyko, D. Hlushkou, S. Khirevich, and U. Tallarek, *J. Chromatogr. A* **1257**, 98 (2012).
- [84] U. M. Scheven, S. Khirevich, A. Daneyko, and U. Tallarek, *Phys. Rev. E* **89**, 053023 (2014).
- [85] W. Feller, *An Introduction to Probability Theory and Its Applications* (John Wiley & Sons, New York, 1968).
- [86] G. Taylor, *Proc. R. Soc. Lond. A* **219**, 186 (1953).
- [87] R. Aris, *Proc. R. Soc. Lond. A* **235**, 67 (1956).
- [88] D. A. Edwards, M. Shapiro, H. Brenner, and M. Shapira, *Transp. Porous Media* **6**, 337 (1991).
- [89] A. Eidsath, R. G. Carbonell, S. Whitaker, and L. R. Herrmann, *Chem. Eng. Sci.* **38**, 1803 (1983).
- [90] G. Chiogna, C. Eberhardt, P. Grathwohl, O. A. Cirpka, and M. Rolle, *Environ. Sci. Technol.* **44**, 688 (2010).
- [91] Y. Ye, G. Chiogna, O. Cirpka, P. Grathwohl, and M. Rolle, *J. Contamin. Hydrol.* **172**, 33 (2015).
- [92] M. L. Porter, F. J. Valdés-Parada, and B. D. Wood, *Adv. Water Resour.* **33**, 1043 (2010).
- [93] M. Rolle, D. Hochstetler, G. Chiogna, P. K. Kitanidis, and P. Grathwohl, *Transp. Porous Media* **93**, 347 (2012).
- [94] D. L. Hochstetler, M. Rolle, G. Chiogna, C. M. Haberler, P. Grathwohl, and P. K. Kitanidis, *Adv. Water Resour.* **54**, 1 (2013).
- [95] Y. Liu and P. K. Kitanidis, *Adv. Water Resour.* **62**, 303 (2013).
- [96] J. Crank, *The Mathematics of Diffusion* (Clarendon Press, Oxford, 1975).
- [97] C. Song, P. Wang, and H. A. Makse, *Nature* **453**, 629 (2008).
- [98] B. S. Everitt and A. Skrondal, *The Cambridge Dictionary of Statistics* (Cambridge University Press, Cambridge, 2010).
- [99] T. Müllner, K. K. Unger, and U. Tallarek, *New J. Chem.* **40**, 3993 (2016).